



Composition and Properties of Aspirin Through DFT Analysis

Rebaz A. Omer*, Zainab A. Omer, Sada M. Hassan

Koya University, Faculty of Science & Health, Department of Chemistry, Koya KOY45, Kurdistan Region – F.R.

*Corresponding author: Rebaz OMER email: rebaz.anwar@koyauniversity.org

ABSTRACT

Computing research on aspirin has produced considerable knowledge of its molecular structure and actions. It has revealed its chemical characteristics and connections with other molecules. Data from the study will be used to further investigate the effects of the drug and potential new uses for it. Using Density Functional Theory (B3LYP/cc-pVDZ) computations, we analyzed the optimal molecular shape, vibrational frequencies, ¹H- and ¹³C-NMR chemical shifts. We also investigated electronic structural factors, such as dipole moment (μ), hardness (η), softness (σ), electronegativity (χ), electrophilicity index (ω), nucleophilicity index (ϵ), and chemical potential (Π), which are connected to corrosion inhibition efficacy. Additionally, we calculated the fraction of transferred electrons (ΔN) to determine the interaction between the iron surface and organic molecules. The calculations revealed a positive association between organic-based corrosion inhibitors and quantum chemical parameters processes. Thus, the behavior of corrosion inhibitors can be predicted without the need for experimental investigation.

ARTICLE INFO

Keywords:

Materials Science
IR spectroscopy
NMR spectroscopy
DFT

Received: 2023-10-14

Accepted: 2023-11-20

ISSN: 2651-3080

DOI: 10.54565/jphcfum.1375349

I ntroduction

Acetylsalicylic acid (ASA), commonly known as aspirin, is an odorless, colorless to white, crystalline powder with the chemical formula $C_9H_8O_4$. It is one of the most widely used medications and is a gentle and effective antipyretic and sedative that is used as an analgesic for less severe pains, anti-inflammatory, and anti-platelet effects. Its first applications of decoctions or preparations of plants containing salicylate can be traced back to thousands of years ago [1, 2]. Aspirin is known to double the likelihood of living a long life. It was discovered that salicylic acid and acetyl chloride interacted to form ASA [3, 4]. Aspirin and other non-steroid anti-inflammatory medications (NSAIDs) reduce the activity of the cyclooxygenase (COX) enzyme, resulting in the production of prostaglandins (PGs) responsible for pain, inflammation, edema, and fever. However, the aspirin-like medications also hinder the generation of physiologically significant PGs that shield the stomach mucosa from harm by HCl by blocking this crucial enzyme in PG synthesis. Additionally, aspirin is known to have anticoagulant properties and its used [5-7].

In 1897, Felix Hoffman, an employee of the Bayer company in Germany, synthesized acetylated salicylic acid, which was then marketed under the brand name "Aspirin", and went on

to become the most popular medication ever [5, 8]. Studies have shown that these compounds possess both phyto- and chemotherapeutic properties, and in recent years there has been considerable research into Aspirin's antiproliferative and anticancer properties [9, 10]. Since its first use as a pain reliever, Aspirin has been widely employed due to its wide range of applications in general medicine, cardiovascular medicine, neurology, obstetrics and gynecology, dentistry, gastrointestinal and oncology [11].

Aspirin is available in various forms, including tablets, powders, and oral gels. It is a commonly prescribed antiplatelet drug that works by irreversibly inhibiting the cyclooxygenase 1 (COX1) enzyme, thus preventing platelet activation and aggregation by reducing the formation of prostaglandin G_2/H_2 and thromboxane A_2 (TXA₂) [12, 13]. Aspirin is used to relieve pain, reduce fever, reduce swelling, and in populations where colon, prostate, and breast cancers are common, long-term use of adult-strength aspirin may be associated with a modest decrease in overall cancer incidence [14]. It can also help to prevent heart attack, angina, stroke, transient ischemic attack (TIA), peripheral arterial disease (PAD), coronary artery bypass surgery, or other heart or blood vessel-related operations. Aspirin decreases a patient's chances of developing recurrent

colorectal adenomas in the near future. Common side effects of short-term aspirin use include headaches, migraines, toothaches, period pain, general aches and pains, and cold and flu symptoms [15].

Using the methods of DFT, a study of Aspirin was conducted. The results of this research were quite illuminating, providing information about the chemical composition of the drug and how it might interact with other substances. Additionally, the study explored the various physical and chemical properties of Aspirin, giving insight into its potential applications. This research was a valuable contribution to our understanding of this common drug.

Computational Study

Density functional theory (DFT) is a powerful tool for studying the stability and reactivity of chemical species, and synthetic organic chemists can make decisions about which chemical transformations will take place in reactions using computational chemistry tools. Gaussian 09 and the Gauss View 5 program [16, 17] were used to optimize the geometric structures of the molecule in the gas phase and calculate its vibrational frequency in order to obtain the theoretical infrared spectra [18-20]. Using the (RB3LYP/CC-pVDZ) level of theory, the title molecule's reactivity was determined based on the energy values of its highest occupied molecular orbital (HOMO) and lowest unoccupied molecular orbital (LUMO). [21, 22]. The energy gap (En gap) between the LUMO-HOMO orbitals can be used to predict the chemical reactivity of a species, with low reactivity indicated by large values of (En gap) and high reactivity shown by short values of (En gap) [23-25].

$$E_{n \text{ gap}} = E_{\text{LUMO}} - E_{\text{HOMO}} \quad [23] \quad (1)$$

The Koopmans' DFT theorem proposes a relationship between the ionization energy (I) and the electron affinity (A) of a chemical compound with the energy of the HOMO orbital (Eq. 2) and the energy of the LUMO orbital (Eq. 3) respectively [26-28].

$$I = -E_{\text{HOMO}} \quad [26] \quad (2)$$

$$A = -E_{\text{LUMO}} \quad [26] \quad (3)$$

The chemical properties of electronegativity (χ), chemical potential (μ), and global chemical hardness (η) can be understood through DFT theory as derivatives of the molecule's electronic energy (E) relative to the sum of all its electrons (N) at a fixed external potential (ν). Mathematically this is expressed as: $\chi = -\partial E/\partial N$; $\mu = \partial E/\partial N$; and $\eta = 2\partial^2 E/\partial N^2$ [29-31].

$$\chi = -\mu = \left(\frac{\partial E}{\partial N}\right)\nu \quad [30] \quad (4)$$

$$\eta = \frac{1}{2} \left(\frac{\partial^2 E}{\partial N^2}\right)\nu \quad [30] \quad (5)$$

According to Iczkowski and Margrave [32], the electronegativity and chemical potential of a given atom or molecule can be expressed as a function of the ionization energy and electron affinity (Eq. (6)). Further, Janak's theorem and the valence state parabola model can be employed to determine the global chemical hardness (Eq. (5)) as outlined in [33, 34].

Global softness (S), (Eq. (6)), is the reciprocal of global chemical hardness.

$$S = \frac{1}{\eta} \quad [35] \quad (6)$$

The global electrophilicity index (ω), proposed by [36], is a measure of a chemical species' propensity to receive electron density (atom, molecule, or ion). The greater the value of ω , the more electrophilic the species is; conversely, the lower the value of ω , the more nucleophilic the species is. This inverse measure is referred to as the nucleophilicity (ε) [37, 38].

$$\omega = \frac{\mu^2}{4\eta} \quad [37] \quad (7)$$

$$\omega = \frac{\chi^2}{2\eta} \quad [37] \quad (8)$$

$$\varepsilon = \text{Pi. } \eta \quad [37] \quad (9)$$

Results and Discussions

Geometrical analysis

The DFT/CC-pVDZ approach was employed to optimize the chemical's molecular structure, and the results revealed that the molecule's structural properties in the gaseous phase were ideal. Table 1 displays the computed structural characteristics related to the molecule's stable state as well as the Aspirin molecule. Aspirin consists of an aromatic ring (C1-C2-C3-C4-C5-C6) and a carboxylic group (C11-O13-O12-H14) along with an ester group (C16-O17-C18-H19-H20-H21) as seen in Figure 1. The bond length between the atoms in the aromatic double bond is close, with a value of 1.39 Å. Similarly, the bond length for (H7-C2), (H8-C3), (H9-C4) (H10-C5) is close, at 1.09 Å, due to the fact that they are all linked to carbons in the aromatic ring, (C11-C6) and (C18-C16) have similar bond lengths, 1.49 Å and 1.05 Å, respectively. As for (O12-C11) and (O13-C11), the former has a different bond length of 1.21 Å compared to the latter with 1.36 Å due to the difference in the type of bond formed; O12 forms a double bond with C11 while O13 forms a single bond with C11. The smallest bond length is that of (H14-O13) at 0.98 Å, which is due to oxygen being the more electronegative atom. The largest bond angle is (O12-C11-C6) while the smallest is (H14-C13-C11) at 123.6359° and 104.6451°, respectively. The dihedral angles

were calculated using the Gaussian 09 program, as mentioned in Table 1.

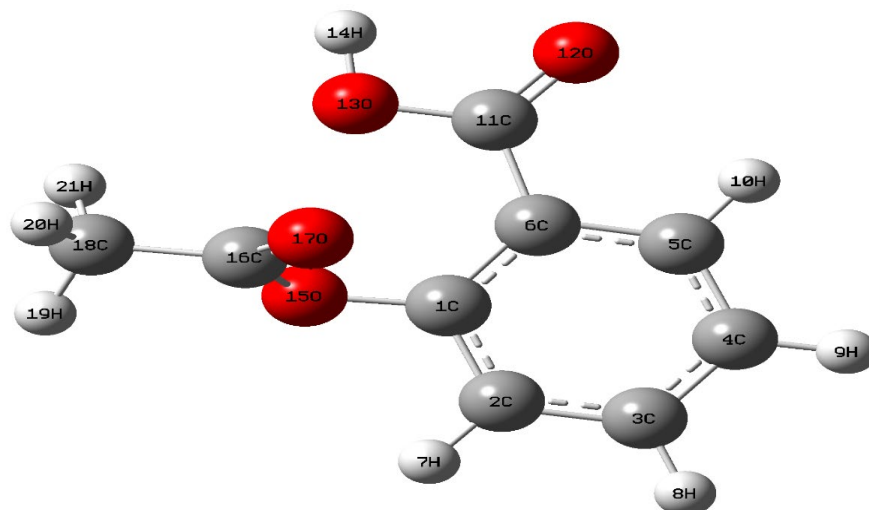


Fig. 1 Geometrical structure of Aspirin

Table 1. Bond Length, bond angle and Dihedral angle for Aspirin

Symbol	Bond	Symbol	Angle	Symbol	Dihedral
C2-C1	1.3955199	C3-C2-C1	120.3883	C4-C3-C2-C1	0.311903
C3-C2	1.3947905	C4-C3-C2	119.9366	C5-C4-C3-C2	-0.31916
C4-C3	1.3986219	C5-C4-C3	119.5385	C6-C5-C4-C3	0.071629
C5-C4	1.3916014	C6-C5-C4	121.4853	H7-C2-C1-C6	-179.809
C6-C5	1.4067983	H7-C2-C1	118.2929	H8-C3-C2-C1	-179.934
H7-C2	1.0908867	H8-C3-C2	119.6593	H9-C4-C3-C2	179.8636
H8-C3	1.0921872	H9-C4-C3	120.4133	H10-C5-C4-C3	-179.816
H9-C4	1.091518	H10-C5-C4	121.2592	C11-C6-C5-C4	-179.133
H10-C5	1.0903117	C11-C6-C5	115.6663	O12-C11-C6-C5	-2.21251
C11-C6	1.4933366	O12-C11-C6	123.6359	O13-C11-C6-C5	177.1784
O12-C11	1.2136353	O13-C11-C6	115.0607	H14-C13-C11-C6	179.3865
O13-C11	1.3555927	H14-C13-C11	104.6451	O15-C1-C2-C3	176.6294
H14-O13	0.975226	O15-O1-C2	116.8328	C16-O15-C1-C2	104.0517
O15-C1	1.3885405	C16-O15-C1	118.1178	O17-C16-O15-C1	-5.08319
C16-O15	1.3824647	O17-C16-O15	123.3087	C18-C16-O15-C1	174.985
O17-C16	1.2010481	C18-C16-O15	109.4012	H19-C18-C16-O15	50.02247
C18-C16	1.5036763	H19-C18-C16	110.4897	H20-C18-C16-O15	172.2266
H19-C18	1.0999814	H20-C18-C16	109.6777	H21-C18-C16-O15	-67.5717
H20-C18	1.0962249	H21-C18-C16	108.5504		
H21-C18	1.1011184				

O: oxygen, H: Hydrogen

Infrared (IR) Spectroscopy

Periodic density functional theory (DFT) using the (RB3LYP/ CC-pVDZ) method in combination with FTIR spectroscopy in the 4000–400 cm^{-1} range [39, 40] was used to analyze the FT-IR spectrum of Aspirin. The C=O symmetrical stretching (1858.42 cm^{-1} , 1802.40 cm^{-1}) of (C16=O17), (C11=O12) was the two strongest peaks and the C-O frequency of (C11-O13), (C1-O15), (C11-O13) was

1388.09 cm^{-1} , 1238.63 cm^{-1} , 1128.63 cm^{-1} respectively as shown in Figure 2 and Table 2, The O-H vibration was detected above 3703 cm^{-1} . Additionally, different frequencies were observed for the same atom in the Aspirin molecule vibration, such as 1221.92, 1203.35 for (C11-O13, C16-O15) and 1105.04 for (C11-O13, C1-O15), which were all symmetrical stretching at strong peaks.

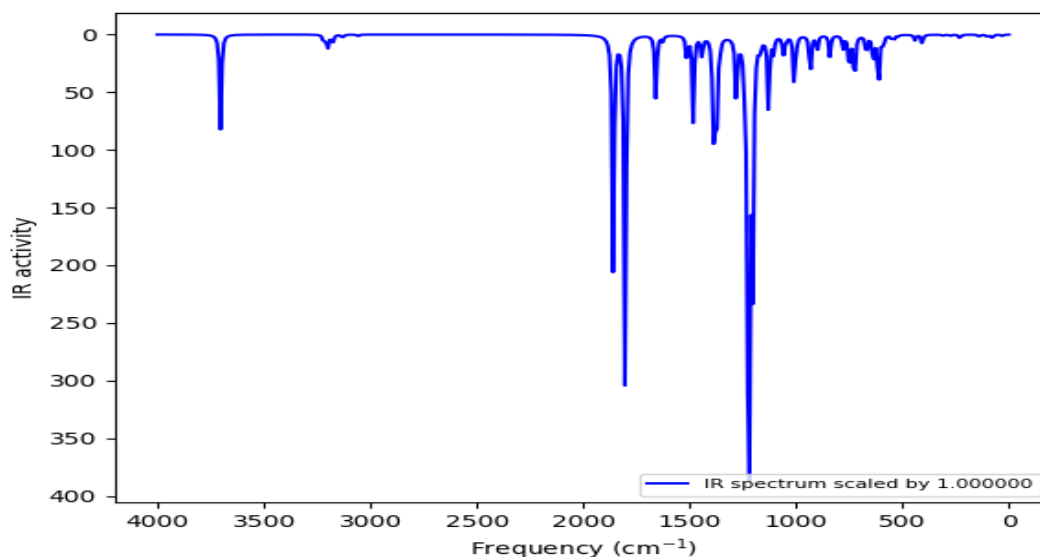


Fig. 2 FT-IR spectrum of Aspirin

Table 2. Vibration Spectrum of Aspirin

Atoms Vibration	Frequencies (RB3LYP/ CC-pVDZ)
(O13 – H14) _{STV}	3703.01
(C5- H10) _{STV}	3220.34
(C3- H8, C2-C7) _{STV}	3210.46
(C4-H9, C3-H8) _{STV}	3199.55
(C3-H8 , C4-H9) _{UNSTV}	3183.98
(CH3) _{USTV}	3174.24
(C18-H19- H21) _{UNSTV}	3130.14
(C18-H19-H20-H21) _{STV}	3057.11
(C16=O17) _{STV}	1858.42
(C11= O12) _{STV}	1802.40
(C1=C2, C4=C5 ARO) _{STV}	1658.19
(C4=C3, C1=C6 ARO) _{STV}	1625.93
(C-H in Ring) _{RO}	1512.49
(C3-H8,C4-H9,C1,C6 in Ring) _{RO}	1482.45
(C18- H19-H20-H21) _{SCI}	1444.51
(C18-H19-H21) _{SCI}	1439.9
(C11-O13) _{STV}	1388.09
(C18- H19-H20-H21) _{WA}	1374.43
(C=C ARO) _{STV}	1358.71
((H7,H8,H9,H10 ARO),O13-H14) _{RO}	1280.08
(C1-O15) _{STV}	1238.63
(C11-O13 ,C16-O15) _{STV}	1221.92
(C11-O13 ,C16-O15) _{STV}	1203.35
(C-H ARO) _{SCI}	1167.41
(C11-O13) _{STV}	1128.63
(C11-O1 , C1-O15) _{STV}	1105.04
(C3 - C4 ARO) _{STV}	1059.51
(C16-C18) _{STV}	1046.71
(C-H ARO) _{TW}	1017.15
(C16-C18) _{STV}	1007.75
(C-H ARO) _{TW}	993.55

TV: Starching vibration, UN: anti, S: Symmetrical, RO: Rocking, SCI: Scissoring, TW: Twisting, WA: Wagging.

Nuclear magnetic resonances (^1H and ^{13}C -NMR)

The structure of organic molecules can be ascertained using the method known as NMR spectroscopy (nuclear magnetic resonance spectroscopy). It has been demonstrated that quantum chemical calculations are enough for forecasting NMR spectra and examining the relationship between

molecule structure and chemical shifts. [41, 42]. The title chemical's geometry was optimized using the standard gauge-including atomic orbital (GIAO) method, and the ^1H and ^{13}C NMR spectra were estimated using the RB3LYP/CC-pVDZ methodology and the Gaussian 09 program. The ^1H -NMR chemical shifts ranged from 0.00 to 9.00 ppm see Figure 3.

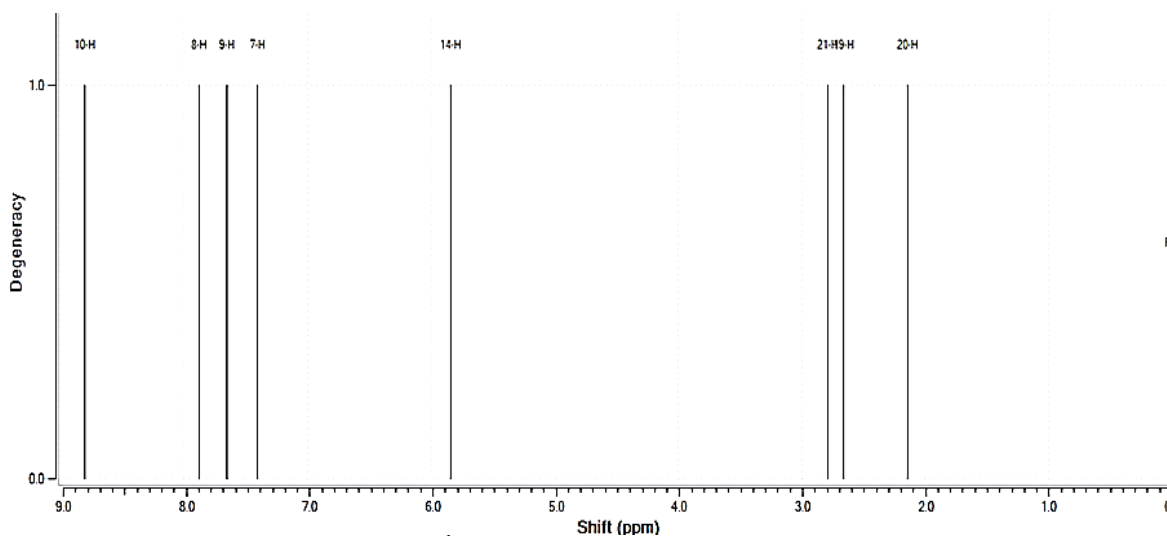


Fig. 3 ^1H NMR spectrum for the Aspirin

^1H -NMR was used to determine that the chemical shift values for (Ar - H) above 7 ppm, (H-10) has a higher shift value which (8.8 ppm), and the lowest field depends on it near higher electronegativity of the carbonyl group, (H-7), **Table 3.** Chemical shifts (ppm) of ^1H -NMR of the ASA.

(H-9) and (H-8) depend not effected by any groups they have shifted nearly value which (7.40 - 7.66-7.88) ppm, respectively, and (H-14) shifted to (5.86), see Table 3.

^1H -number	Results
H-10	8.80
H-8	7.88
H-9	7.66
H-7	7.40
H-14	5.84
H-21	2.79
H-19	2.66
H-20	2.14

The RB3LYP/CC-pVDZ approach using the Gaussian 09 program was used to find the compound ^{13}C -NMR resonance signals in the gas phase between 11.58 and 155.14 ppm, see Figure 4. Using ^{13}C -NMR, it was found that the chemical shift values of the (C-16) are (155.14 ppm) which is higher shifted depending on the electronegativity of oxygen, (C-11)

value is (150.71 ppm) depending on the carbon of the carbonyl group, (C-1) is shifted to (143.30 ppm) which depends on bonded with (O-15) which has more electronegativity, and chemical shift value of (C-6), see Table 4.

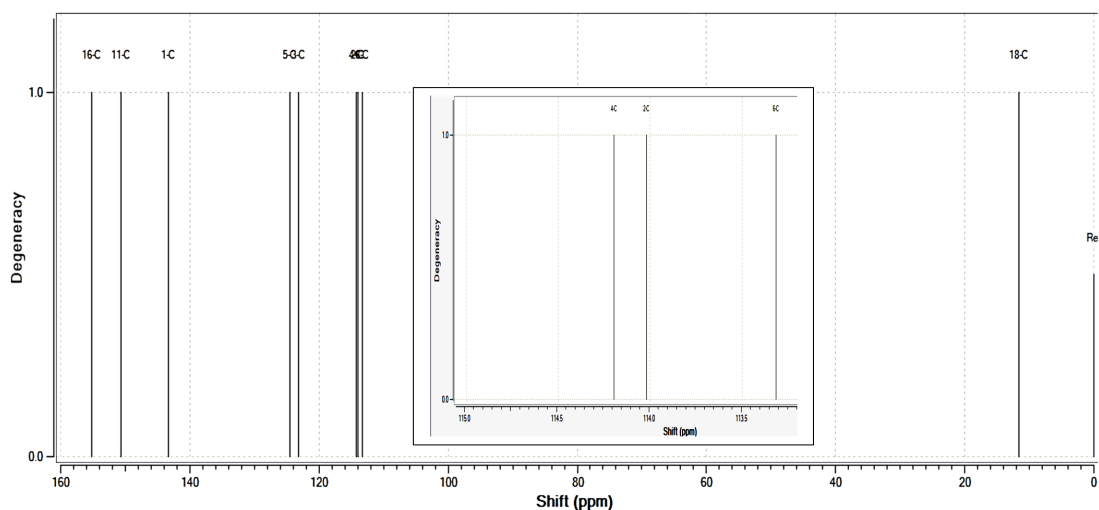


Fig. 4 ^{13}C -NMR spectrum for the Aspirin

Table 4. Chemical shifts (ppm) of ^{13}C -NMR of the ASA

^{13}C -Number	Results
C-16	155.14
C-11	150.71
C-1	143.30
C-5	124.51
C-3	123.14
C-4	114.20
C-2	114.02
C-6	113.31
C-18	11.58

HUMO – LUMO Energy Level

The energy difference between the highest occupied molecular orbital (HOMO) and the lowest occupied molecular orbital (LUMO), commonly referred to as the band-gap, is a crucial factor in determining the chemical stability of a molecule. The size of this band-gap has significant effects on the molecule's electrical and optical properties, as well as its electronic absorption spectra [43]

The RB3LYP/ CC-pVDZ technique was used to calculate the HOMO and LUMO energies of the molecule in the gas phase, which resulted in values of (-7.153 eV) and (-1.786 eV), respectively. The difference between these energies, also known as the band-gap, was (- 5.367 eV). Figure 5 presents 3D plots of the HOMO and LUMO. Additionally, the Gauss Sum 3.0 software was employed to determine the density of states (DOS) of the compound in the gas phase, and the results are shown in Figure 6.

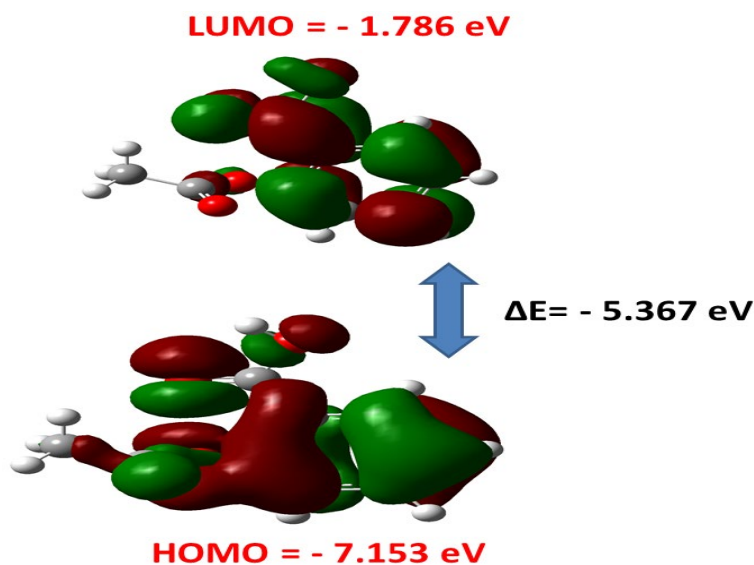


Fig. 5 Energy level HOMO-LUMO of Aspirin

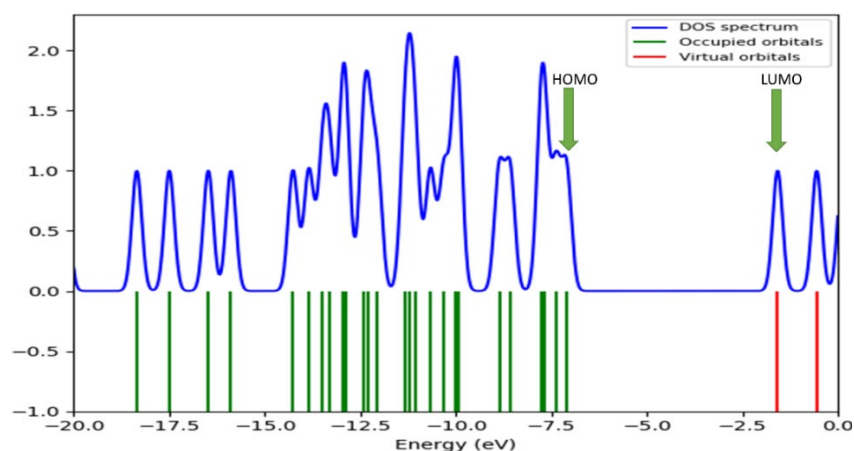


Fig. 6 Depicting Diagrams the density states for the Aspirin.

The electrostatic surface potential (ESP)

The electrostatic surface potential (ESP) is a visual method for understanding the relative polarity of compounds [44-46]. As shown in Figure 7, the electrostatic surface potential (ESP) map illustrates the charge distribution of the molecule in a 3D representation. The surface used for this map is based on the constant electron density of either the highest occupied molecular orbital (HOMO) or the total electron density, which helps to identify the reactive site of the molecule. This is a valuable tool, as it allows for the visualization of molecular size, shape, and areas of electrostatic potential energy through color coding, thereby facilitating an understanding of the relationship between molecular structure and physical and chemical properties [47, 48]. The color grading used in the mapped electrostatic surface potential (ESP) depicts potential increases in the order of red, orange, yellow, green, and blue. The charge

distributions obtained from ESP maps can be used to predict molecule-molecule interactions. In these maps, blue regions represent positive electrostatic potentials, green regions indicate near zero potentials, and red regions denote negative potentials, with the intensity inversely proportional to the potential energy's absolute value. Figure 7 visually represents the chemically active sites and relative reactivity of atoms. In the case of SP/MC, blue indicates the strongest attraction, while red denotes the strongest repulsion. Regions of negative value are typically associated with the lone pair of electronegative atoms. The distribution of electronegativity in the Aspirin molecule was observed between oxygen atoms numbered twelve and seventeen in Figure 7. The blue area in the Aspirin molecule was located between hydrogen atoms numbered eight, indicating a greater degree of ionization due to a wider range of electronegativity. Overall, the electrostatic potential map

surface and Millikan charge distribution on the molecule

surface in Figure 8 revealed these findings.

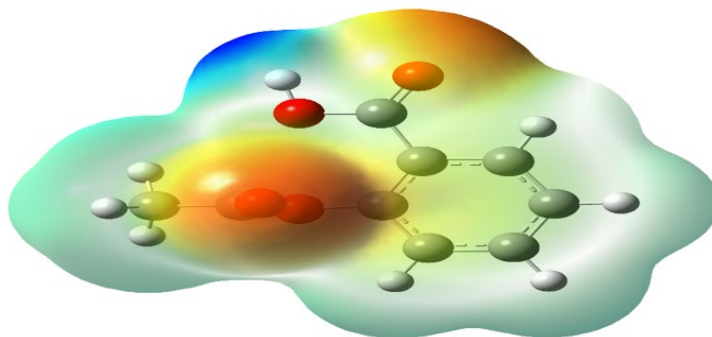


Fig. 7 The electrostatic surface potential (ESP) for Aspirin.

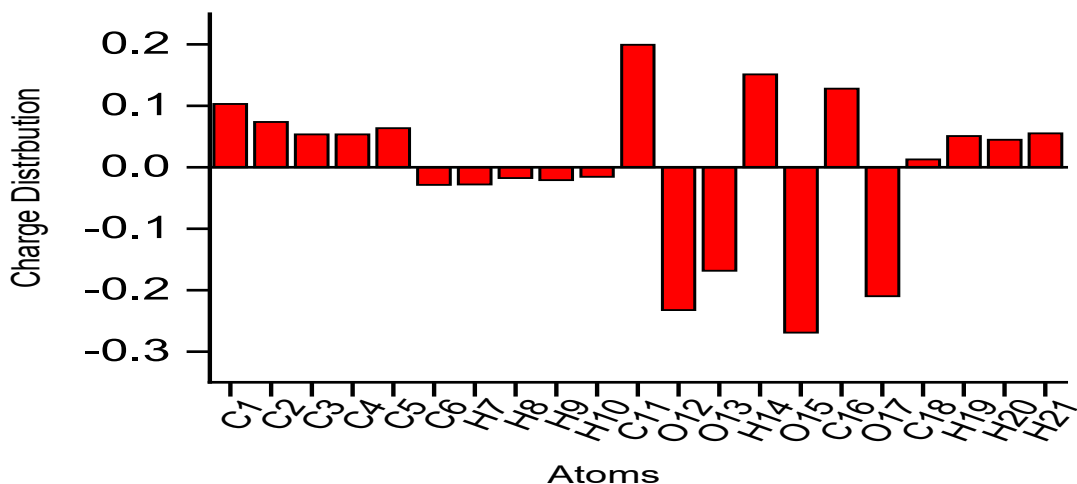


Fig. 8 Millikan atoms charge distribution of Aspirin.

UV–VIS spectra analysis

The analysis of Aspirin's ultraviolet spectrum has been studied by theoretical computation. By using the DFT/RB3LYP in Gaussian program by using CC-pVDZ Basis Set, approach, the absorption maxima (max) (nm) for the molecule's lower-lying singlet states have been

computed. Figure 9 lists the predicted oscillator strength, excitation energies, and absorption maxima which is (258.513 nm), the absorbance maxima of this molecule correlate to the electron transition between border orbitals, like translation from HOMO, according to calculations of the molecular orbital geometry [49].

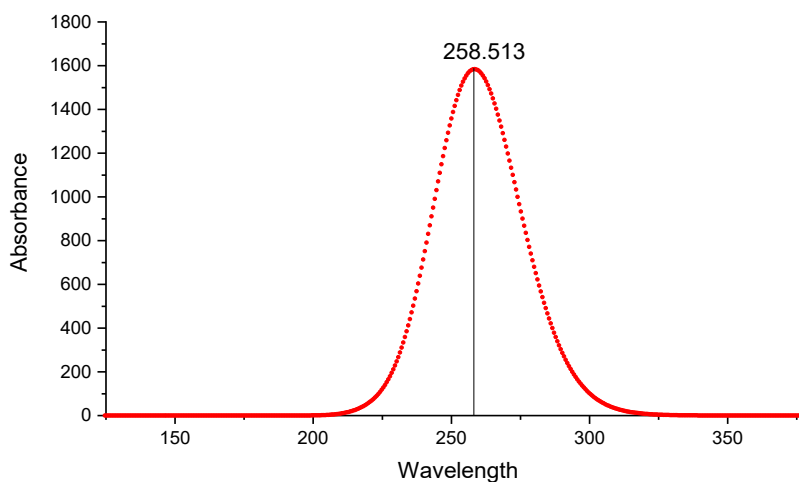


Fig. 9 UV–VIS spectrum of Aspirin

Study of Inhibitor Activity

Various molecular structural factors such as HOMO and LUMO energy levels, energy bandgap (ΔE), χ , η , σ , ω , P_i , ϵ , and μ play a vital role in determining the electronic structure of a compound. The Gaussian output file is used to obtain these parameters including HOMO, LUMO, and other values. Furthermore, Koopman's theorem can also be used in this regard [26, 50, 51]. According to Koopman's theorem, the EHOMO and ELUMO values of a molecule are linked to its ionization energy and electron affinity values. The electrophilicity index (ω) is a measure of the total energy depletion caused by the transfer of electrons between the transmitter and receiver. The nucleophilicity index (ϵ) is a new identifier for chemical structures, and the equation (ΔN) is used to calculate the number of electrons transferred between the inhibitor and the metal surface. Using the B3LYP/cc-pVDZ method, the HOMO and LUMO energies of the 22 compounds in question were theoretically calculated and found to be -7.153 eV and -1.786 eV, respectively. The high HOMO energy of the molecule results in a greater inhibitory capacity, while the low LUMO energy values lead to the inhibitor producing a negative charge on the metal surface. As a result, the compound has the strongest corrosion inhibition activity, as evidenced by its high HOMO and low LUMO energy values [52-56]. Overall, the title compound has the strongest corrosion inhibition activity due to its high HOMO and low LUMO energy values.

The Mulliken atomic charge distribution [50-52] Determining the adsorption sites of inhibitors is a commonly used method, and many researchers have suggested that the presence of negatively charged heteroatoms can enhance the potential for these atoms to adsorb onto metal surfaces through the donor-acceptor process [42, 57, 58]. The electrostatic potential map surface in Figure 8 reveals that approximately 25% of the atoms in the inhibitor molecule are negatively charged, which implies that the compound has

robust anti-corrosive characteristics. To assess the inhibitor's stability, reactivity, and activity, the hardness and softness parameters (η and σ) should be considered. Organic inhibitors based on Lewis acids are typically classified as soft inhibitors, which means they are more reactive than hard inhibitors and therefore exhibit stronger anti-corrosive properties [59].

Our findings indicate that compounds with high EHOMO and low ΔE values have higher softness and lower hardness. The values of η and σ provided in Table 5 indicate that the chemical in question has the most effective inhibition activity. To assess inhibitor activity, we also considered the variables electronegativity (χ) and chemical potential (P_i). Our calculations revealed how the metal and inhibitor form a coordinated covalent bond. This study focused on the corrosion inhibition behavior of a compound used as an iron metal inhibitor. Experimentally, we observed that the (χ) value of the iron bulk metal was higher than the (χ) value for the inhibitor listed in Table 5, indicating that the iron metal could form bonds by absorbing electrons from the inhibitor molecule. Since the compound inhibitor has a higher (χ) value, it is the most effective corrosion inhibitor compared to the literature [60, 61]. Table 5 lists the dipole moment (μ) property, but its relationship with inhibitory activity has not been established in previous research. Some experiments have suggested that molecules with higher dipole moment values have stronger inhibitory activity, while others have shown that inhibitory effect decreases with lower dipole moment values [62, 63]. Our compound exhibits a dipole moment of 2.46 Debye. The effectiveness of corrosion inhibitors can be determined using two important measures - the electrophilicity index (ω) and the nucleophilicity index (ϵ). The ω value of an inhibitor molecule indicates its ability to receive electrons, whereas its ϵ value indicates its ability to donate electrons. An increase in the ϵ value corresponds to an increase in inhibition activity, while a decrease in the ω value leads to a reduction in inhibition activity [64, 65]. According to our findings, the ϵ value of our molecule has

increased while the ω value has decreased, indicating that our compound has strong inhibitory activity. The ΔN results from Table 5 further support this conclusion, as the molecule

is capable of transferring additional electrons to the surface of iron metal, making it a highly effective inhibitor.

Table 5. Calculation quantum chemical parameters for Aspirin

Parameters	Results
Total Energy (a.u)	-648.74
$\mu(D)$	2.46
E_{LUMO} (eV)	-1.786
E_{HOMO} (eV)	-7.153
En gap (eV)	-5.367
I	7.153
A	1.786
χ (eV)	4.47
η (eV)	2.68
σ (eV)	2.67
Pi (eV)	- 4.47
ω (eV)	1.67
ε (eV)	-11.98
ΔN	-0.18

Conclusion

Gaussian 09 software was utilized to optimize the compound's geometry and perform theoretical FT-IR, 1H -, and ^{13}C NMR spectroscopy. Additionally, Mulliken atomic charges, HOMO-LUMO energies, and a molecular electrostatic potential (MEP) map were obtained at the B3LYP/ccpVDZ level of theory. The calculated HOMO and LUMO energies (-5.367eV) suggest inhibitory activity of the molecule. 3D graphs of the HOMO and LUMO showed charge transfer from the benzene ring to the aliphatic part. Using the Mulliken population method, positive charge distributions were found on the atoms in the molecule, particularly the electronegative atoms, which are believed to significantly impact inhibitory efficacy. The MEP study revealed the most negative potential site on the O12, O13, O15, and O17 atoms, with the most positive potential around the hydrogen atoms. The values of η , ω , σ , ε , Pi, and χ indicate that the title chemical is a potent inhibitor. Increasing ΔN is expected to enhance the corrosion effect by promoting better absorption on the metal surface. This research provides valuable insights into the design, synthesis, and corrosion activity of new materials, particularly the compound under investigation. Computational methods were employed to study aspirin's chemical properties and interactions, yielding significant results that enhance our understanding of the drug's molecular structure and behavior. The data collected from this study will contribute to exploring potential new applications of aspirin. Gaussian 09 software was utilized to generate the compound's optimal geometry. Theoretical FT-

IR, 1H -, and ^{13}C -NMR spectroscopy results were presented, as well as Mulliken atomic charges, HOMOLUMO energies, and MEP map at the B3LYP/ccpVDZ level of theory. The HOMO and LUMO energies were determined to be -5.367eV, indicating that the molecule has inhibitory activity. 3D graphs of the HOMO and LUMO showed the charge transfer from the benzene ring to the aliphatic part. The Mulliken population method was used to calculate the charge distributions of the molecule, with positive charge distributed on the atoms in a molecule. Electronegative atoms were believed to have a significant impact on inhibitory efficacy when taking into consideration the atomic charges of a compound inhibitor. The molecular electrostatic potential (MEP) study revealed the most negative potential site to be on the O12, O13, O15 and O17, and the most positive potential site around the hydrogen atoms. The values of η , ω , σ , ε , Pi and χ suggest that the title chemical has the strongest inhibitor. An increase in more ΔN will further raise the corrosion effect due to better absorption on the surface of the metal. This research is expected to assist in the design, synthesis, and corrosion activity of new materials, such as the compound. The chemical properties and interactions of aspirin have been studied using computational methods. The research has yielded significant results, offering valuable insight into the molecular structure and behavior of the drug. The data collected from the study will be utilized to expand our understanding of aspirin's effects and explore potential new applications.

ACKNOWLEDGEMENTS

Acknowledging Support from Koya University's Department of Chemistry

CONFLICT OF INTEREST

The authors declare that they have no conflicts of interest.

REFERENCES

- M.F. Khan, R.B. Rashid, and M.A. Rashid, Computational study of geometry, molecular properties and docking study of aspirin. *World J Pharm Res*, 2015. **4**: p. 2702-2714.
- G. Pasero and P. Marson, A short history of anti-rheumatic therapy. II. Aspirin. *Reumatismo*, 2010. **62**(2): p. 148-156.
- G. Adebayo, J. Williams, and S. Healy, Aspirin esterase activity—Evidence for skewed distribution in healthy volunteers. *European Journal of Internal Medicine*, 2007. **18**(4): p. 299-303.
- A.B. Moreira, et al., Solid-phase fluorescence spectroscopy for the determination of acetylsalicylic acid in powdered pharmaceutical samples. *Analytica chimica acta*, 2004. **523**(1): p. 49-52.
- J. Vane and R. Botting, The mechanism of action of aspirin. *Thrombosis research*, 2003. **110**(5-6): p. 255-258.
- B. Campbell, Anticoagulation for patients with arterial disease. *European Journal of Vascular and Endovascular Surgery*, 2001. **21**(1): p. 1-2.
- E.S. Huang, et al., Long-term use of aspirin and the risk of gastrointestinal bleeding. *The American journal of medicine*, 2011. **124**(5): p. 426-433.
- O. Rebaz, R.F. Rashid, and K. OTHMAN, Exploring The Synthesis of 1, 2, 4-Triazole Derivatives: A Comprehensive Review. *Journal of Physical Chemistry and Functional Materials*. **6**(1): p. 43-56.
- J. Mahdi, et al., The historical analysis of aspirin discovery, its relation to the willow tree and antiproliferative and anticancer potential. *Cell proliferation*, 2006. **39**(2): p. 147-155.
- M.J. Desborough and D.M. Keeling, The aspirin story—from willow to wonder drug. *British journal of haematology*, 2017. **177**(5): p. 674-683.
- M. Ugurlucan, et al., Aspirin: from a historical perspective. *Recent Patents on Cardiovascular Drug Discovery (Discontinued)*, 2012. **7**(1): p. 71-76.
- T.E. Wallen, et al., Aspirin Administration Mitigates Platelet Hyperaggregability After Splenectomy in a Murine Model. *Journal of Surgical Research*, 2022. **279**: p. 548-556.
- S. Dutta and P. Sengupta, Men and mice: relating their ages. *Life sciences*, 2016. **152**: p. 244-248.
- E.J. Jacobs, et al., A large cohort study of long-term daily use of adult-strength aspirin and cancer incidence. *Journal of the National Cancer Institute*, 2007. **99**(8): p. 608-615.
- E. Flossmann and P.M. Rothwell, Effect of aspirin on long-term risk of colorectal cancer: consistent evidence from randomised and observational studies. *The Lancet*, 2007. **369**(9573): p. 1603-1613.
- L. Wilbraham, C. Adamo, and I. Ciofini, Communication: evaluating non-empirical double hybrid functionals for spin-state energetics in transition-metal complexes. *The Journal of chemical physics*, 2018. **148**(4): p. 041103.
- A. Vektariene, G. Vektaris, and J. Svoboda, A theoretical approach to the nucleophilic behavior of benzofused thieno [3, 2-b] furans using DFT and HF based reactivity descriptors. *Arkivoc: Online Journal of Organic Chemistry*, 2009.
- E. Cancès, B. Mennucci, and J. Tomasi, A new integral equation formalism for the polarizable continuum model: Theoretical background and applications to isotropic and anisotropic dielectrics. *The Journal of chemical physics*, 1997. **107**(8): p. 3032-3041.
- T. Risthaus and S. Grimme, Benchmarking of London dispersion-accounting density functional theory methods on very large molecular complexes. *Journal of chemical theory and computation*, 2013. **9**(3): p. 1580-1591.
- L. AHMED and O. Rebaz, Population Analysis and UV-Vis spectra of Dopamine Molecule Using Gaussian 09. *Journal of Physical Chemistry and Functional Materials*, 2020. **3**(2): p. 48-58.
- D.H. Pereira, et al., New perspectives on the role of frontier molecular orbitals in the study of chemical reactivity: a review. *Revista Virtual de Quimica*, 2016: p. 425-453.
- B. Kumar, et al., Crystal structure of 1-(4-fluorophenyl)-4-(4-methoxyphenyl)-1H-1, 2, 3-triazole. *Acta Crystallographica Section E: Crystallographic Communications*, 2015. **71**(Pt 8): p. o534.
- K. Fukui, Role of frontier orbitals in chemical reactions. *science*, 1982. **218**(4574): p. 747-754.
- L. AHMED and O. Rebaz, Spectroscopic properties of Vitamin C: A theoretical work. *Cumhuriyet Science Journal*, 2020. **41**(4): p. 916-928.
- I. Obot, D. Macdonald, and Z. Gasem, Density functional theory (DFT) as a powerful tool for designing new organic corrosion inhibitors. Part 1: an overview. *Corrosion Science*, 2015. **99**: p. 1-30.
- T. Koopmans, Über die Zuordnung von Wellenfunktionen und Eigenwerten zu den einzelnen Elektronen eines Atoms. *physica*, 1934. **1**(1-6): p. 104-113.
- S.Y. Omar, et al., Investigating the Role of Metoclopramide and Hyoscine-N-Butyl Bromide in Colon Motility. *ARO-THE SCIENTIFIC JOURNAL OF KOYA UNIVERSITY*, 2023. **11**(2): p. 109-115.

28. H.H. Rasul, et al., Theoretical investigation on corrosion inhibition efficiency of some amino acid compounds. *Computational and Theoretical Chemistry*, 2023: p. 114177.
29. H. Chermette, Chemical reactivity indexes in density functional theory. *Journal of computational chemistry*, 1999. **20**(1): p. 129-154.
30. R.G. Parr and R.G. Pearson, Absolute hardness: companion parameter to absolute electronegativity. *Journal of the American chemical society*, 1983. **105**(26): p. 7512-7516.
31. L. AHMED, et al., Quantum Chemical Study of Some Basic Organic Compounds as the Corrosion Inhibitors. *Journal of Physical Chemistry and Functional Materials*, 2023. **6**(1): p. 34-42.
32. L.H. Madkour, et al., Quantum chemical calculations, molecular dynamic (MD) simulations and experimental studies of using some azo dyes as corrosion inhibitors for iron. Part 2: Bis-azo dye derivatives. *Journal of Molecular Structure*, 2018. **1163**: p. 397-417.
33. J.F. Janak, Proof that $\partial \epsilon / \partial n_i = \epsilon_i$ in density-functional theory. *Physical Review B*, 1978. **18**(12): p. 7165.
34. L. Von Szentpály, Studies on electronegativity equalization: part 1. Consistent diatomic partial charges. *Journal of Molecular Structure: THEOCHEM*, 1991. **233**: p. 71-81.
35. W. Yang and R.G. Parr, Hardness, softness, and the Fukui function in the electronic theory of metals and catalysis. *Proceedings of the National Academy of Sciences*, 1985. **82**(20): p. 6723-6726.
36. H. Raissi, et al., Relationships between experimental and theoretical scales of electrophilicity of 7-L-4-nitrobenzofurazans. *Journal of Molecular Structure*, 2021. **1224**: p. 128843.
37. A. Toro-Labbé, *Theoretical aspects of chemical reactivity*. 2006: Elsevier.
38. M.M. Marinho, et al., Quantum computational investigations and molecular docking studies on amentoflavone. *Heliyon*, 2021. **7**(1): p. e06079.
39. C.O. Areán, et al., Computational and Fourier transform infrared spectroscopic studies on carbon monoxide adsorption on the zeolites Na-ZSM-5 and K-ZSM-5: evidence of dual-cation sites. *The Journal of Physical Chemistry C*, 2008. **112**(12): p. 4658-4666.
40. V. Arjunan and S. Mohan, Fourier transform infrared and FT-Raman spectra, assignment, ab initio, DFT and normal co-ordinate analysis of 2-chloro-4-methylaniline and 2-chloro-6-methylaniline. *Spectrochimica Acta Part A: Molecular and Biomolecular Spectroscopy*, 2009. **72**(2): p. 436-444.
41. L. AHMED and O. Rebaz, A theoretical study on Dopamine molecule. *Journal of Physical Chemistry and Functional Materials*, 2019. **2**(2): p. 66-72.
42. O. Rebaz, et al., Theoretical Determination of Corrosion Inhibitor Activities of Naphthalene and Tetralin. *Gazi University Journal of Science*, 2022: p. 1-1.
43. G.Ö. Tarı, S. Gümüş, and E. Açar, Crystal structure, spectroscopic studies and quantum mechanical calculations of 2-[(3-iodo-4-methyl)phenylimino]methyl]-5-nitrothiophene. *Spectrochimica Acta Part A: Molecular and Biomolecular Spectroscopy*, 2015. **141**: p. 119-127.
44. J.S. Murray and P. Politzer, The electrostatic potential: an overview. *Wiley Interdisciplinary Reviews: Computational Molecular Science*, 2011. **1**(2): p. 153-163.
45. D.M. Mamad, R.A. Omer, and K.A. Othman, Quantum chemical analysis of amino acids as anti-corrosion agents. *Corrosion Reviews*, 2023(0).
46. D.M. Mamad, et al. *Insight into Corrosion Inhibition Efficiency of Imidazole-Based Molecules: A Quantum Chemical Study*. in *Doklady Physical Chemistry*. 2023. Springer.
47. V.I. Minkin, et al., Spectroscopic and theoretical evidence for the elusive intermediate of the photoinitiated and thermal rearrangements of photochromic spiropyran. *The Journal of Physical Chemistry A*, 2005. **109**(42): p. 9605-9616.
48. G. Cottone, R. Noto, and G. La Manna, Theoretical study of spiropyran-merocyanine thermal isomerization. *Chemical Physics Letters*, 2004. **388**(1-3): p. 218-222.
49. M. Abdel-Mottaleb and S.N. Ali, A new approach for studying bond rupture/closure of a spiro benzopyran photochromic material: reactivity descriptors derived from frontier orbitals and DFT computed electrostatic potential energy surface maps. *International Journal of Photoenergy*, 2016. **2016**.
50. R. Anwar Omar, et al., A novel cyclobutane-derived thiazole-thiourea hybrid with a potency against COVID-19 and tick-borne encephalitis: synthesis, characterization, and computational analysis. *Journal of Sulfur Chemistry*, 2023: p. 1-18.
51. P. Koparir, et al., Novel 1, 2, 4-triazolethiol-thiophen Hybrids: Facile Synthesis, Characterization, ADMET Prediction and Molecular Docking. *Polycyclic Aromatic Compounds*, 2023: p. 1-15.
52. R.A. Omar, et al., A novel coumarin-triazole-thiophene hybrid: synthesis, characterization, ADMET prediction, molecular docking and molecular dynamics studies with a series of SARS-CoV-2 proteins. *Journal of Chemical Sciences*, 2023. **135**(1): p. 6.
53. R.A. Omer, P. Koparir, and M. Koparir, Synthesis, experimental and theoretical characterization with inhibitor activity for 1, 2, 4-triazol derivatives. *Indian Journal of Chemistry (IJC)*, 2022. **61**(12): p. 1278-1287.

54. R. Omer, et al., Synthesis, Characterization and DFT Study of 1-(3-Mesityl-3-methylcyclobutyl)-2-((4-phenyl-5-(thiophen-2-yl)-4H-1, 2, 4-triazol-3-yl) thio) ethan-1-one. *Protection of Metals and Physical Chemistry of Surfaces*, 2022: p. 1-13.
55. A.E. Parlak, et al., Experimental, DFT and Theoretical Corrosion Study for 4-(((4-ethyl-5-(thiophen-2-yl)-4H-1, 2, 4-triazole-3-yl) thio) methyl)-7, 8-dimethyl-2H-chromen-2-one. *Arabian Journal of Chemistry*, 2022. **15**(9): p. 104088.
56. P. Koparir, et al., Synthesis, Characterization and Computational Analysis of Thiophene-2, 5-Diylbis ((3-Mesityl-3-Methylcyclobutyl) Methanone). *Polycyclic Aromatic Compounds*, 2022: p. 1-19.
57. Z. El Adnani, et al., DFT theoretical study of 7-R-3methylquinoxalin-2 (1H)-thiones (RH; CH₃; Cl) as corrosion inhibitors in hydrochloric acid. *Corrosion science*, 2013. **68**: p. 223-230.
58. R.A. Omer, P. Koparir, and L.O. Ahmed, Characterization and inhibitor activity of two newly synthesized thiazole. *Journal of Bio-and Tribo-Corrosion*, 2022. **8**(1): p. 28.
59. D. Alexander and A. Moccari, Evaluation of corrosion inhibitors for component cooling water systems. *Corrosion*, 1993. **49**(11).
60. S. Martinez, Inhibitory mechanism of mimosa tannin using molecular modeling and substitutional adsorption isotherms. *Materials chemistry and physics*, 2003. **77**(1): p. 97-102.
61. R.M. Issa, M.K. Awad, and F.M. Atlam, Quantum chemical studies on the inhibition of corrosion of copper surface by substituted uracils. *Applied Surface Science*, 2008. **255**(5): p. 2433-2441.
62. S. Chen, et al., Quantum chemical study of some benzimidazole and its derivatives as corrosion inhibitors of steel in HCl solution. *Int. J. Electrochem. Sci*, 2014. **9**: p. 5400-5408.
63. M. Beytur, et al., Synthesis, characterization and theoretical determination of corrosion inhibitor activities of some new 4, 5-dihydro-1H-1, 2, 4-Triazol-5-one derivatives. *Heliyon*, 2019. **5**(6): p. e01809.
64. N. Karakus and K. Sayin, The investigation of corrosion inhibition efficiency on some benzaldehyde thiosemicarbazones and their thiole tautomers: Computational study. *Journal of the Taiwan Institute of Chemical Engineers*, 2015. **48**: p. 95-102.
65. S. Erkan, K. Sayın, and D. Karakaş, Theoretical studies on eight oxovanadium (IV) complexes with salicylaldehyde and aniline ligands. *Hacettepe J Biol Chem*, 2014. **42**: p. 337-342.